Journal of Materials Chemistry C

Accepted Manuscript

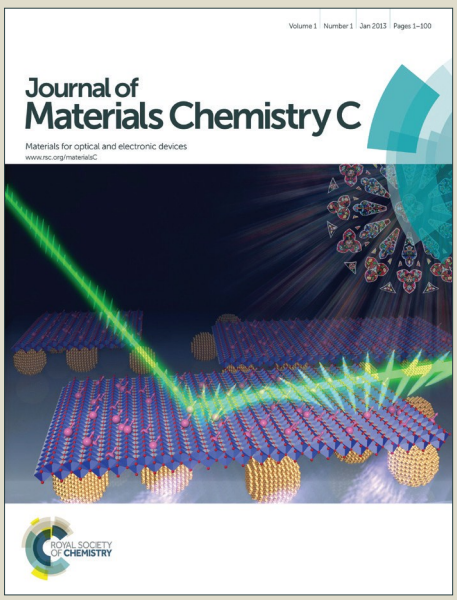

ROYAL SOCIETY OF CHEMISTRY

www.rsc.org/materialsC

Lead Free Relaxor Ferroelectric Ceramics with High Optical Transparency and Energy Storage Ability

Bingyue Qu[1], Hongliang Du[2], Zetian Yang[2],

[1]College of Physics, Jilin University, Changchun, 130012, China

[2]Science College, Air Force Engineering University, Xi'an 710051, China

Abstract:

We have attained high transparent relaxor ferroelectric ceramics based on $(K_{0.5}Na_{0.5})NbO_3$ prepared using pressure-less solid-state sintering method, without using hot isostatic pressing and spark plasma sintering. Both the energy storage density of 2.48 J/cm^3 and high transparency in the visible spectra (~60 % at 0.7μm) were achieved at $0.8(K_{0.5}Na_{0.5})NbO_3$-$0.2Sr(Sc_{0.5}Nb_{0.5})O_3$ ceramics with submicron sized grains (about 0.5μm). The energy storage density of 2.48 J/cm^3 exceeds all other reported result of lead-free bulk ceramics. The results demonstrate that the $0.8(K_{0.5}Na_{0.5})NbO_3$-$0.2Sr(Sc_{0.5}Nb_{0.5})O_3$ ceramics were promising lead-free transparent dielectric materials for transparent electronic devices applications. This study not only open up a new avenue to design lead free transparent ferroelectric ceramics with high energy storage density but also expands the applications of $(K_{0.5}Na_{0.5})NbO_3$ based ceramics into new areas beyond piezoelectric applications.

Keywords: transparent electronic devices, energy storage, relaxor, lead free, $(K_{0.5}Na_{0.5})NbO_3$,

Introduction

Transparent electronic devices have attracted considerable attention since its tendency of being the potential candidate for the next generation of electronic devices because of their great potential to make intensive research interest and significant commercial impact in consumer electronic products such as e-readers, smart phones and touch panels.[1-6] Recently, a wide range of transparent electrical components, including conducting elements and circuitry, capacitors, diodes, transistors, audio speakers, and sensors, have been developed.[7-13] Among those applications, energy storage component plays an important role in electric energy storage and power generation, the transparent pulsed capacitors still have not been developed owing to the absence of transparent dielectric materials with high energy storage density.

Transparent pulsed capacitors (TPC) require dielectric materials should possess not only high energy storage density but also well optically transparent in the visible range. However, conventional dielectric materials can not satisfy above requirements at the same time. Currently, there are two major types of conventional dielectric materials for pulsed capacitors: ceramics and polymers.[14-18] Polymer dielectric materials usually possess high energy density owing to their high dielectric breakdown strength (DBS). However, polymer dielectric materials are limited to relatively low working temperatures range (< 105 ℃), and thus fail to meet the rising demand for electricity under the extreme fields.[19] In contrast, ceramic dielectric materials exhibit superior mechanical and thermal properties, and are thus considered the potential best candidate for the pulsed capacitor applications. Nevertheless, it usually is difficult to fabricate transparent dielectric ceramics using pressure-less solid-state sintering method, except for transparent

ceramics (Pb, La)(Zr, Ti)O_3, because dielectric ceramics have various sites to scatter light such as rough surface, residual pores at the grain boundaries, grain boundaries, second phases (impurities) at the grain boundaries and double refraction from birefringent materials.[20] Although (Pb, La)(Zr, Ti)O_3 ceramics show good transparent, these materials contain more than 60 wt % lead. In recent years, some countries have required all new electronic products to be lead-free for the environmental protection and human health reasons.[21] Therefore, it is desirable to develop lead-free transparent dielectric ceramics with high energy storage density to fabricate transparent pulsed capacitor.

Generally speaking, in order to achieve high optical transparence lead free ceramics, a widely adopted strategy is to eliminate all possible scattering sites of light, which requires conditions as follows: high density, absence of pores (or the pores size is smaller than the wavelength of light), absence of second phase(impurity), small grain size (be close to the wavelength of visible light), isotropic lattice structure and surface as smooth as possible.[20] Among these important factors, the grain size play a key role in determining optical transparence of ceramics, for that the size of pores at grain boundary becomes to be smaller than the wavelength of light when the grain size is close to it, resulting in quickly reducing the dispersion of the pores, the grains and the grain boundaries. Several studies have confirmed that ferroelectric ceramics with the grain size around the visible wavelength can show good optical transparence.[22, 23] For example, Wu et al reported that the spark plasma-sintered ($Ba_{0.5}Sr_{0.5}$)TiO_3 ceramics have a high transparency (~74 % at 0.623μm) owing to few pores and small grain sizes (0.88μm).[22] Liu et al. had synthesized lead-free transparent $BaTiO_3$ and $SrTiO_3$ ceramics by spark plasma sintering, and these ceramics have small grain size (from 0.1μm-0.5μm) and excellent optical transparency in

both visible and infrared wavelength ranges.[23] However, to the best of our knowledge, there are not yet any reports on energy storage properties of lead-free transparent $BaTiO_3$ and $SrTiO_3$ ceramics. Based on above discussion, we think that it is possible to achieve high optical transparence ferroelectric ceramics by reducing the grain size of lead-free ferroelectric ceramics to submicron scale (be close to the wavelength of the visible light). Currently, the fabrication methods of ferroelectric ceramics with submicron sized grains are mostly hot-pressure sintering or spark plasma sintering. These methods have two disadvantages, namely, they are incapable of preparing the samples with particular figured, and need high production cost during the preparing. Consequently, the pressure-less solid-state sintering is expected to replace hot-pressure sintering or spark plasma sintering in fabricating ceramics with submicron sized grains.

In recent years, a number of studies on lead free ceramics have focused on improving the piezoelectric and dielectric properties of $(K_{0.5}Na_{0.5})NbO_3$(KNN)-based ceramics.[24-28] In those studies, one result should be noteworthy that the addition of secondary compound can obviously reduce the grain size of KNN-based ceramics from micron order to submicron, without using hot-pressure sintering or spark plasma sintering. For example, the grain size of KNN-$BiScO_3$ ceramics decrease from 10-20 μm for pure KNN ceramics to 1 μm for 0.96KNN-0.04$BiScO_3$ ceramics.[29] Marija et al. reported that the grain size of KNN-$SrTiO_3$ ceramics decreased to the submicron size with the increase of $SrTiO_3$ content.[30] Suh a characteristic of KNN-based ceramics may lead to good transparency. As a result, Li et al. reported that Li and Bi co-modified $(K_{0.5}Na_{0.5})NbO_3$ ceramics possess high transparency (60 % at a wavelength of 0.8μm) owing to the effective suppression of grain growth.[31] Our group also found that

$0.95(K_{0.5}Na_{0.5})NbO_3$-$0.05Ba(Sc_{0.5}Nb_{0.5})O_3$ ceramics exhibit 54% transparence in the visible spectra.[32] However, the studies on electric energy storage properties of such KNN-based lead free ceramics have not yet been reported in the open literatures.

In the present work, we report our recent advance on transparent ferroelectric ceramics which are based on $(K_{0.5}Na_{0.5})NbO_3$-$Sr(Sc_{0.5}Nb_{0.5})O_3$ (KNN-SSN) ceramics prepared using pressure-less solid state sintering method. Figure 1 shows schematic diagram of increasing optical transparency and energy storage density by decreasing the grain size of KNN-SSN ceramics in this study. In our results, both high optical transparency in the visible spectra and large energy storage density were achieved at 0.8KNN-0.2SSN ceramics. Such results demonstrate that 0.8KNN-0.2SSN ceramic is promising lead-free transparent dielectric materials for transparent electronic devices applications.

Experimental

Materials preparation: $(1-x)(K_{0.5}Na_{0.5})NbO_3$-$xSr(Sc_{0.5}Nb_{0.5})O_3$ (x =0, 0.04, 0.06, 0.08 0.1, 0.2 and 0.3) ceramics in this study were fabricated by conventional solid-state reactions. Reagent-grade oxides and carbonate powders of K_2CO_3, Na_2CO_3, Sc_2O_3, $SrCO_3$ and Nb_2O_5 were used as starting raw materials. They were milled for 24 h using planetary milling with 2-5 mm diameter zirconia ball media and alcohol. The slurry was dried at 120 °C prior to calcination. Calcination was performed in an alumina crucible that was heated at 950 °C for 5 h. A twice calcinations process was used in this study to achieve pure perovskite structure, the calcined powders were ground, calcined at 950 ◦C for 5 h again. Then these powders were ball milled again in the same manner as above for 12 h. After drying the powder, these powers were mixed with 5 wt% solution of PVA as a

binder. The sample were pressed into plate-shape of 15mm×15mm×1mm in length, breadth and thickness under 300 MPa. After burning off PVA, the samples were sintered at 1200–1300 ◦C for 5 h soaking period in air in covered alumina crucibles. In order to suppress the high volatilization of alkali metal oxides at a high temperature during sintering, a double crucible method was used in this study.[33] For electrical measurements, the sintered samples were polished to achieve parallel and smooth faces with a thickness of 0.2-0.5 mm prior to the application of silver paste. In order to prevent the samples edge breakdown, the silver paste with 6 mm ×6 mm was screen printed by mesh screen mask of 200 lines per inch on the both surfaces of the samples as electrode. A silver electrode was obtained by firing at 820°C for 20 min.

Characterization: The transmittance of the ceramics was measured using a UV–Vis spectrophotometer (UV-2550; Shimadzu Co., Tokyo, Japan).The phase structures of the sintered ceramics were examined using an X-ray diffractometer (Philips X-Pert ProDiffractometer, Almelo, the Netherlands). The microstructure of the ceramic samples was observed using scanning electron microscopy (SEM, model JSM-6360, JEOL, Tokyo, Japan). The temperature dependence of permittivity was carried out from -200°C to 500°C in custom-designed furnaces with a precision LCR meter (E4980A; Agilent, Palo Alto, CA) over a frequency range from 1 kHz to 1 MHz. The polarization–electric field (P–E) hysteresis loops were measured at ambient temperature at 1 Hz using a ferroelectric test system (TF Analyzer 2000; aixACCT, Aachen, Germany).

Results and Discussion

Figure 2a shows the transparency of the (1-x)KNN-xSSN (x=0.2 and 0.3) ceramics

polished to a thickness of 0.3 mm. The letters can be clearly read through the samples, suggesting that (1-x)KNN-xSSN (x=0.2 and 0.3) ceramics have good transparencies in the visible spectra. Within the measured wavelength range, 0.8KNN-0.2SSN ceramic shows broad transmission spectra starting from 0.37μm, and the transmission is close to 60% in the visible spectra, and about 70% at the near-infrared wavelengths. Several researchers found that the right way to confirm the transparency of transparent ceramics is to maintain a sufficiently large distance between the objects and the transparent samples.[34] Figure 3b shows a photograph of a highly transparent 0.8KNN-0.2SSN ceramics where the background behind (the flower and building) can be easily seen through the sample. High transmittance of the 0.8KNN-0.2SSN ceramic can be attributed to submicron-sized grains (the average grain size of 0.5μm), which is comparable to the wavelength of light. This result will be discussed in later section.

Crystal structure plays an important role in determining the optical transmittance of ferroelectric ceramics.[17] The ceramics with a cubic perovskite structure generally have high optical transmittance, for that the scattering of light is small at the grain boundaries with isotropic lattice structure when the light travels from one grain to another. However, ferroelectric ceramics usually possess non-cubic phase structure such as rhombohedral, tetragonal, orthorhombic ferroelectric phases at room temperature, so the scattering of light is strong at the grain boundaries during the transmission of light. This is the reason why most ferroelectric ceramics generally are opaque. Therefore, transparent ferroelectric ceramics usually should possess pseudo-cubic phase to synchronously obtain high optical transmittance and ferroelectric properties.

Figure 3 is the X-ray diffraction (XRD) patterns of (1-x)KNN-xSSN ceramics record

ed at room temperature, which show that, all samples with x from 0.0 to 0.30 possess pure perovskite phase, without any secondary phase. This indicates that the SSN have completely diffused into the KNN lattice forming a new solid solution. The orthorhombic phase is characterized by (202) / (020) peak splitting about 45°. The cubic phase is characterized by single (200) peak about 45°.[30] From figure 4b, one can see that the split (202)/(020) peaks gradually disappear as the increase of SSN content, which indicates that the phase structure of (1-x)KNN-xSSN ceramics is pure perovskite phase with orthorhombic symmetry at x =0.0 and 0.04, the pseudo-cubic phase at x=0.08, 0.10 and 0.2, and the cubic phase at x= 0.30. The lattice constants of (1-x)KNN-xSSN ceramics as a function of the SSN content are shown in Figure 4.This can be explained as follows: for the ABO_3 perovskite structure, Sr^{2+} possesses the different valence and ionic radii with Na^+ and K^+ in the A sites, Sc^{3+} and Nb^{5+} bring the distortion formation of the structural framework and the phase structure transition by occupying the B sites. This interpretation also can be confirmed by subsequent dielectric spectrums.

Figure 5 shows is the scanning electron microscopy (SEM) micrographs obtained from the surface of (1-x)KNN-xSSN samples sintered at the optimum sintering temperature. It should be clearly observed that the addition of SSN compound can remarkably inhibit the growth of grains of KNN-SSN ceramics. The average grain size of the (1-x)KNN-xSSN specimen are about 4-8μm, 0.5μm and 0.4μm for x=0.0, 0.2 and 0.3, respectively. In addition, both the cases of x=0.2 and 0.3 are highly dense due to that there are very few residual open pores can be discerned; if any, the diameter is smaller than 0.1μm or so. Especially for the case of x=0.2, the grain size (about 0.5μm) and its distribution is uniform, which are in favor of obtaining good transparency in the visible

spectra (~60% at 0.7μm). To further appreciate the stoichiometry characterization of (1-x)KNN-xSSN ceramics after the sintering, energy dispersion spectrum analysis (EDS) was used to confirm the atomic percentages of the elements of (1-x)KNN-xSSN ceramics. Figure 6 shows the surface morphologies, EDS spectra and atomic percentages of the elements of pure KNN and 0.8KNN-0.2SSN ceramics. The Na/K ratio of (1-x)KNN-xSSN (x=0 and 0.2) ceramics become large after the sintering than initial stoichiometry characterization due to high volatilization of potassium at a high sintering temperature.

Ferroelectric ceramics with submicron sized grains only can be fabricated using several special fabrication techniques, such as hot isostatic pressing and spark plasma sintering. However, those methods require costly equipment and are not suitable for industry production. In this study, compositions drive the grain size of (1-x)KNN-xSSN ceramics to submicron scale, without using hot isostatic pressing and spark plasma sintering. This result confirms the relaxor ferroelectric ceramics with submicron sized grains could be prepared using pressure-less solid-state sintering through the control of compositions.

Figure 7 shows the temperature dependence of dielectric permittivity of (1-x)KNN-xSSN ceramics at a temperature range of -200-500 °C, where the measuring frequency was chosen at 1 MHz to eliminate space-charge polarization contributions at high temperatures and lower measurement frequency. For pure KNN ceramics, two sharp dielectric peaks can be observed at 190°C and 397°C, which correspond to the phase transitions from orthorhombic to tetragonal and from tetragonal to cubic, respectively. Whereas for $x \geq 0.10$, only a dielectric peak is observed at the examined temperature

range. The ferroelectric-paraelectric phase transition temperatures, namely, the maximum dielectric permittivity temperature (T_m), decreases from 397 °C for the pure KNN ceramics to 305 °C , 217 °C, 58 °C, -112 °C and -164 °C for the ceramics, when x=0.04, x=0.08, x=0.10, x=0.20 and x=0.30, respectively. This result confirms the change of the phase structure in the KNN-SSN solid solution with increasing SSN content at room temperature, and is consistent with above XRD analysis shown by Figure 4. Moreover, the phase transition temperature range around T_m become wider with increasing addition of SSN, which confirms the existing of diffuse phase transition, a typical characteristic for the relaxor ferroelectrics.

Another typical characteristic for the relaxor ferroelectrics is the frequency dispersion of the dielectric permittivity. Figure 8 shows the temperature dependence of dielectric permittivity of (1-x)KNN-xSSN ceramics at various measuring frequencies. For pure KNN ceramics, the dielectric permittivity is nearly frequency independence, which indicates that pure KNN ceramic is a normal ferroelectric. Whereas for KNN-SSN, for instance x=0.10, a strong frequency dispersion of dielectric permittivity and the diffuse phase transition are observed. As the two typical characteristics for the relaxor ferroelectrics, the simultaneous presence of the diffuse phase transition and the frequency dispersion of dielectric permittivity indicate that 0.90KNN-0.10SSN ceramics are indeed lead-free relaxor ferroelectrics.

The relaxational behavior in relaxor ferroelectrics can be explained by many theory models such as composition fluctuation theory, superparaelectricity theory, the model of the merging micropolar regions into macropolar regions, and the model of random-field, etc.，A common point of these models is based on the local distortion of the crystal

structure, giving rise to polar nano-regions (PNRs). Analyzing the local distortion of the crystal structure, K^+ and Na^+ occupy the equivalent crystallographic sites (A-site) in pure KNN solid solutions, but the disorder in the perovskite structure does not appear because K^+ has the same valence as Na^+, and thus is not in favor of the formation of local order-disorder of the crystal structure. whereas in the solid solution of 0.90KNN-010SSN, Na^+, K^+ and Sr^{2+} occupy the A sites of ABO_3 perovskite structure because of their large ionic radius, and Sr^{2+} possesses the different valence and ionic radii with Na^+ and K^+, which result in the formation of the local electric fields owing to the local charge imbalance and the local elastic fields due to local structure distortions. The similar phenomenon also occurs at B-sites of ABO_3 perovskite structure, where Sc^{3+} and Nb^{5+} also possess the different valence and ionic radii. Additionly, the influences from the random-fields cannot be ignored. In (1-x)KNN-xSSN, the local electric fields and the elastic fields, will give rise to the PNRs by hindering the long-range dipole alignment. Hence, it is reasonable to conclude that the long range ferroelectric order cannot form in the (1-x)KNN-xSSN due to the existing of PNRs. However, the emergence of the large amount of PNRs can result in the formation of the pseudocubic phase and decrease the optical anisotropy, which can decrease the scattering of light at the grain boundaries, and thus bring optical transparence to ferroelectric ceramics with relaxor behavior.

For relaxor ferroelectric ceramics, the electric energy storage density W can be estimated from their P-E hysteresis loops by using the following expression: [35]

$$W = \int_0^{P_{\max}} EdP \qquad (1)$$

Where E is the electric field and P is the polarization. When the electric field increases from zero to the maximum E_{max}, the polarization increases to the maximum

P_{max}, and electric energy is stored in relaxor ferroelectric ceramics, illustrated by the green and red area in Figure 9. During the discharge process, the recoverable energy storage density W_{rec} is then released from E_{max} to zero, represented by the green area, W_{rec} could be calculated according to the equation below:

$$W_{rec} = \int_{P_r}^{P_{\max}} EdP \quad (2)$$

Where P_r is the remanent polarization, consequently, part of the stored energy (the red area) is unrecovered because of the hysteresis loss as shown in Figure 9, which is called energy loss density W_{loss}. In practical application, apart from higher W_{rec} values, larger high energy storage efficiency η is also always desired. The energy storage efficiency η is calculated as the following formula:

$$\eta = \frac{W_{rec}}{W} = \frac{W_{rec}}{W_{rec} + W_{loss}} \times 100\% \quad (3)$$

The energy storage behavior of the (1-x)KNN-xSSN ceramics with different SSN content was investigated by the P–E hysteresis loops. The P–E hysteresis loops at their critical breakdown strength for all the samples were shown in Figure 10, which were measured at 1 Hz until the samples undergone a breakdown. It can be seen clearly from Figure 10 that the dielectric breakdown strength (DBS) was obviously improved with the increase of SSN content. DBS value showed a maximum 295kV/cm in 0.8KNN-0.2SSN ceramics, DBS values of 295 kV/cm are much higher than other lead-free bulk ceramics.

In general, the DBS of ceramics depends on several internal factors (porosity, grain size and introduction of second phase) and external parameters (sample thickness, sample area, and electrode configuration). Among these factors, the grain size and porosity

appear to be two dominant factors in affecting the DBS. Several researches confirmed that the BDS of ferroelectric ceramics increases with the decrease of the grain size. For example, Song et al. [36] reported that the DBS of $Ba_{0.4}Sr_{0.6}TiO_3$ ceramics increased from 114 kV/cm to 243 kV/cm with decreasing the grain size from 5.6μm to 0.5μm, and $Ba_{0.4}Sr_{0.6}TiO_3$ ceramics with the minimum grain size of 0.5μm exhibited the maximum W_{rec} of 1.28J/cm^3. Ye et al. found that the DBS of TiO_2 ceramic with grain size of 0.200 μm was 1096 kV/cm. Instead, the DBS of TiO_2 ceramic with grain size of 10 μm was 350 kV/cm.[37] Therefore, it is conclude that the high DBS of samples were attributed to their denser microstructure and the submicron grain size (about 0.50μm for 0.8KNN-0.2SSN ceramics). Furthermore, it can be seen from Figure 10 that the P-E hysteresis loops became slimmer with increasing addition of SSN. It is well known that another typical characteristic of relaxor ferroelectric ceramics is a slim P-E loop. A slimmer hysteresis loop observed for 0.8KNN-0.2SSN ceramics further confirms the relaxor behavior in 0.8KNN-0.2SSN ceramics. In addition, almost linear P-E relationships can be observed for 0.7KNN-0.3SSN ceramics. The results indicate that the ferroelectric properties of KNN-SSN ceramics are dramatically decreased with the increase of SSN content. From Figure 10（b），P_s and P_r decrease substantially with the increase of SSN content. For example, the P_s and P_r value are 32.7, 28, 27, 16.4, 7.3 μC/cm^2 and 24.6, 16.7, 9.4 ,2.0, 0.2μC/cm^2 for KNN-SSN ceramics with x = 0.04, 0.08, 0.1, 0.20, and 0.30, respectively.

In order to calculate the energy storage properties, the unipolar P–E hysteresis loops of the ceramics were examined. Figure 11 shows the unipolar P–E hysteresis loops of the (1-x)KNN-xSSN ceramics at room temperature. It can be seen from Figure 11 a and b that W and W_{loss} decrease with the increasing of the content of SSN, whereas W_{rec}

increases substantially. The largest W_{rec} of 2.02 J/cm^3 was obtained at 0.8KNN-0.2SSN ceramics under a high electric field (295 kV/cm). A comparison of energy storage properties among some lead-free ceramics was listed in Table I. It can be seen that W_{rec} of 2.02 J/cm^3 is almost two times higher than that of other lead-free bulk ceramics in the literatures.[34-42] In addition, from Figure 11 b, η increases with the increment of SSN content from 10.6% for 0.96KNN-0.04SSN ceramics, to 81.4 % for 0.8KNN-0.2SSN ceramics, to 94% for 0.7KNN-0.3SSN ceramics.

Figure 12 presents the variations of P–E hysteresis loops of 0.80KNN-0.20SSN ceramics at room temperature under different electric fields. The largest polarization increases from 6.3 μC/cm^2 to 16.3 μC/cm^2 with electric fields increasing from 85 kV/cm to 295 kV/cm, which suggests that a much higher energy density can be achieved by improving dielectric strength of the ceramics.

Conclusion

In conclusion, we have successfully fabricated novel ferroelectric ceramics with not only high optical transparency in the visible spectra (~60% at 0.7μm) but also large energy storage density and dielectric breakdown strength (2.48 J/cm^3 under an electric field of 295kV/cm). These results demonstrate that the $0.8(K_{0.5}Na_{0.5})NbO_3$-$0.2Sr(Sc_{0.5}Nb_{0.5})O_3$ ceramics were promising lead-free transparent dielectric materials for transparent electronic devices applications. High optical transparency and good electrical performance of samples were attributed to their denser microstructure and the submicron grain size (about 0.5μm for 0.8KNN-0.2SSN ceramics). These results confirm that the $(K_{0.5}Na_{0.5})NbO_3$-based relaxor ferroelectrics can be regarded as an alternative direction for the development of transparent energy storage

materials.

Acknowledgements

Authors gratefully acknowledge the supports of the National Science Foundation of China (NSFC no. 61331005), Shaanxi Provincial Natural Science Foundation (2013JM6005), and China Postdoctoral Science Foundation Funded Project(2014T71007).

References

(1) K. Nomura, H. Ohta, A. Takagi, T. Kamiya, M. Hirano and H. Hosono, *Nature* 2004, **432**, 488–492.

(2) L. Wang, M. H. Yoon, G. Lu, Y. Yang, A. Facchetti and T. J. Marks, *Nat. Mater.* 2006, **5**, 893–900.

(3) S. Y. Ju, A. Facchetti, Y. Xuan, J. Liu, F. Ishikawa, P. D. Ye, C. W. Zhou, T. J. Marks and D. B. Janes, *Nat. Nanotechnol.* 2007, **2**, 378–384.

(4) E. Artukovic, M. Kaempgen, D. S. Hecht, S. Roth and G. Gruner, *Nano Lett.* 2005, **5**, 757–760.

(5) Q. Cao, S.-H. Hur, Z.-T. Zhu, Y. Sun, C. Wang, M. A. Meitl, M. Shim and J. A. Rogers, *Adv. Mater.* 2006, **18**, 304–309.

(6) P. Gorrn, M. Sander, J. Meyer, M. Kroger, E. Becker, H. H. Johannes, W. Kowalsky and T. Riedl, *Adv. Mater.* 2006, **18**, 738–741.

(7) S.-K. Lee, B. J. Kim, H. Jang, S. C. Yoon, C. Lee, B. H. Hong, J. A. Rogers, J. H. Cho and J.-H. Ahn, *Nano Lett.* 2011, **11**, 4642−4646.

(8) L. Xiao, Z. Chen, C. Feng, L. Liu, Z.-Q. Bai, Y. Wang, L. Qian, Y. Zhang, Q. Li and K. Jiang, *Nano Lett.* 2008, **8**, 4539−4545.

(9) Z. Wu, Z. Chen, X. Du, J. M. Logan, J. Sippel, M. Nikolou, K. Kamaras, J. R. Reynolds, D. B. Tanner and A. F. Hebard, *Science* 2004, **305**, 1273−1276.

(10) S. Sorel, U. Khan and J. N. Coleman, *Appl. Phys. Lett.* 2012, **101**, 103106.

(11) S. Lee, K. Lee, C.-H. Liu, G. S. Kulkarni and Z. Zhong, *Nat. Commun.* 2012, **3**, 1018.

(12) A. Kudo, H. Yanagi, K. Ueda, H. Hosono, H. Kawazoe and Y. Yano, *Appl. Phys. Lett.* 1999, **75**, 2851−2853.

(13) J. Zhang, C. Wang and C, Zhou, *ACS Nano.* 2012, **6,** 7412-7419.

(14) P. Khanchaitit, K. Han, M. R. Gadinski1, Q. Li and Q. Wang, *Nat. Commun.* 2013, **4**, 1-7.

(15) Z. M. Dang, J. K. Yuan, S. H. Yao and R. J. Liao, Adv. Mater. 2013, 25, 6334-6365.

(16) M. S. Cao, X. X. Wang, W. Q. Cao and J. Yuan, J. Mater. Chem. C, 2015, 3, 6589-6599.

(17) Y. Li, W. Q. Cao, J. Yuan, D. W Wang and M. S. Cao, J. Mater. Chem. C, 2015, 3, 9276-9282.

(18) J. Liu, W. Q. Cao, H. B. Jin, J. Yuan, D. Q. Zhang and M. S. Cao, J. Mater. Chem. C, 2015, 3, 4670-4677.

(19) B. J. Chu, X. Zhou, K. L. Ren, B. Neese, M. R. Lin, Q. Wang, F. Bauer and Q. M. Zhang, Science 2006, 313, 334 – 336.

(20) S.F. Wang, J. Zhang, D.W. Luo,F.Gu, D.Y. Tang, Z.L. Dong, G.E.B. Tan, W.X. Que, T.S. Zhang, S. Li and L.B. Kong, *Prog. Solid State Chem.* 2013, **41**, 20-54.

(21) J. Rodel, *J. Am. Ceram. Soc.* 2009, **92**, 1153-1177.

(22) Y. Wu, N. Wang, S. Wu and X. Chen, *J. Am. Ceram. Soc.* 2011, **94**, 1343–1345.

(23) J. Liu, Z. Shen, W. Yao, Y. Zhao and A. Mukherjee, *Nanotechnology* 2010, 21, 075706.

(24) J. Wu, D. Xiao and J. Zhu, *Chem. Rev.* 2015, **115**, 2559−2595.

(25) J. Li, K. Wang, F. Zhu, L. Cheng and F. Yao, *J. Am. Ceram. Soc.* 2014, **97**, 3529–3532.

(26) J. Zhou, K. Wang, F. Yao, T. Zheng, J. Wu, D. Xiao, J. Zhu and J. Li, *J. Mater. Chem. C*, 2015, **3**, 8780-8787.

(27) Z. Liu, H. Fan and M. Li, *J. Mater. Chem. C*, 2015, **3**, 5851-5858.

(28) T. Zheng, J. Wu, X. Cheng, X. Wang, B. Zhang, D. Xiao, J. Zhu, X. Wang and X. Lou, *J. Mater. Chem. C*, 2014, **2**, 8796-8803.

(29) H. Du, W. Zhou, F. Luo, D.Zhu, S. Qu, Y. Li and Z. Pei, *J. Appl. Phys.* 2008, 104, 044104.

(30) K. Marija, V. Bobnar, M. Hrovat, J. Bernard, B. Malic and J. Holc, *J. Mater. Res.* 2004, 19, 1849-1854.

(31) F. Li and K. Kwok, *J. Am. Ceram. Soc.* 2013, **96**, 3557–3562.

(32) B. Wang, X. Tian, Z. Xu, S. Qu and Z. Li, *Acta Phys. Sin.* 2012, 61, 197703.

(33) B. Zhang, J. Wu, X. Cheng, X.Wang, D. Xiao, J. Zhu, X. Wang and X. Lou, ACS Appl. Mater. Interfaces, 2013, 5, 7718-7725.

(34) A. Krell, T. Hutzler and J. Klimke, *J. Eur. Ceram. Soc.* 2009, **29**, 207-221.

(35) X. Hao, *J. Adv. Dielect.* 2013, 3, 1330001.

(36) Z. Song H. Liu, S. Zhang, Z. Wang, Y.Shi, H. Hao, M. Cao, Z. Yao and Z. Yu, *J. Eur. Ceram. Soc.* 2014, **34**, 1209-1217.

(37) Y. Ye, S. C. Zhang, F. Dogan, E. Schamiloglu, J. Gaudet, P. Castro, M. Roybal and M. Joler, C. Christodoulou, *Proc. IEEE Int. Pulsed Power Conf.* 2003, 1, 719-722.

(38) V. S. Puli, D. K. Pradhan, D. B. Chrisey, M. Tomozawa, G. L. Sharma, J. F. Scott and R. S. Katiyar, *J. Mater. Sci.* 2013, **48,** 2151–2157.

(39) T. Wang, L. Jin, C. Li, Q. Hu and X. Wei, *J. Am. Ceram. Soc.* 2015, **98**, 559-566.

(40) J. Ding, Y. Liu, Y. Lu, H. Qian, H. Gao, H. Chen and C. Ma, *Mater. Lette.* 2014, 114,107-110.

(41) Q. Xu, T. Lia, H. Hao, S. Zhang, Z. Wang, M. Cao, Z. Yao and H. Liu, *J. Eur. Ceram. Soc.* 2014, **34**,1209–1217.

(42) L. Luo, B. Wang, X. Jiang and W. Li, *J. Mater. Sci.* 2014, 49, 1659-1665.

(43) J. Ye, Y. Liu, Y. Lu, J. Ding, C. Ma, H. Qian and Z. Yu, *J. Mater. Sci.: Mater. Electron.* 2014, 25, 4632-4637.

(44) B. Wang, L. Luo, X. Jiang, W. Li and H. Chen, *J. Alloys and Compd.* 2014, 585, 14-18.

(45) D. Zheng, R. Zuo, D. Zhang and Y. Li, *J. Am. Ceram. Soc.* **DOI:10.1111/jace.13737**(2015).

(46) Z. Shen, X. Wang, B. Luo and L. Li, *J. Mater. Chem. A*, 2015, **3**, 18146-18153.

Figure Captions

Figure 1 Schematic diagram of increasing optical transparency and energy storage density by decreasing the grain size through compositions driven

Figure 2 Transparency of the (1-x)KNN-xSSN ceramics. (a) Transparency of the 0.8KNN-0.2SSN ceramics polished to a thickness of 0.3 mm. The lower-right inset shows sample photo of the transparent 0.8KNN-0.2SSN and 0.7KNN-0.3SSN ceramics. (b) Photograph of a visibly transparent 0.8KNN-0.2SSN ceramics.

Figure 3 XRD patterns of the (1-x)KNN-xSSN ceramics. (a) XRD patterns and (b) expanded XRD patterns (40°~50°)

Figure 4 Lattice parameters of (1-x)KNN-xSSN ceramics as a function of x.

Figure 5 SEM images of the (1-x)KNN-xSSN ceramics with (a) x=0; (b) x=0.04; (c) x=0.2; (d) x=0.3;

Figure 6 Surface morphologies, EDS spectra, and atomic percentages of the elements of (a) pure KNN ceramics; (b) 0.8KNN-0.2SSN ceramics;

Figure 7 Temperature dependence of dielectric permittivity of (1-x)KNN-xSSN ceramics within a temperature range of -193-500 °C.

Figure 8 Temperature dependence of dielectric permittivity of (1-x)KNN-xSSN ceramics at various measuring frequencies.

Figure 9 Schematic calculations of energy storage properties of relaxor ferroelectric materials.

Figure 10 (a) P–E hysteresis loops at their critical breakdown strength for (1-x)KNN-xSSN ceramics; (b) P_s and P_r of (1-x)KNN-xSSN ceramics.

Figure 11 (a) The calculated energy storage density W and the recoverable energy storage

density W_{rec}; (b) The calculated energy loss density W_{loss} and the energy storage efficiency η.

Figure 12 Variations of P–E hysteresis loops of 0.80KNN-0.20SSN ceramics under different electric fields.

Table I: Comparison of energy storage properties between 0.8KNN–0.2SSN ceramics and other lead free ceramics

Material system	W [J/cm^3]	W_{loss} [J/cm^3]	W_{rec} [J/cm^3]	η [%]	BDS [kV/cm]	Refereence
$(Ba_{0.4}Sr_{0.6})TiO_3$	-	-	1.28	-	243	Song[36]
0.85BZT-0.15BCT	0.94	0.26	0.68	72	170	Puli[38]
0.90BT-0.10BMN	1.18	0.05	1.13	95.8	150	Wang[39]
0.89BNT-0.06BT-0.05KNN	-	-	0.90	-	100	Ding[40]
0.9(0.92NT-0.08BT)-0.1NN	1.08	0.37	0.71	66	70	Xu[41]
0.90BNT-0.10KN	1.42	0.25	1.17	82.3	104	Luo[42]
0.75(0.8BNT-0.2BKT)-0.25ST	-	-	0.97	-	100	Ye[43]
0.94(0.94BNT-0.06BT)-0.06KN	1.24	0.35	0.89	71.8	100	Wang[44]
0.61BF-0.33BT-0.06BMN	2.08	0.52	1.56	75	125	Zheng[45]
0.91BT-0.09BY	0.86	0.15	0.71	82.6	93	Shen[46]
0.80KNN-0.20SSN	2.48	0.46	2.02	81.4	295	This work

BZT: $Ba(Zr_{0.2}Ti_{0.8})O_3$; BCT: $(Ba_{0.7}Ca_{0.3})TiO_3$; BT: $BaTiO_3$; BMN: $Bi(Mg_{2/3}Nb_{1/3})O_3$; KNN: $(K_{0.5}Na_{0.5})NbO_3$; KN: $KNbO_3$; BNT: $(Bi_{0.5}Na_{0.5})TiO$; BKT: $(Bi_{0.5}K_{0.5})TiO$; ST: $SrTiO_3$; BF : $BiFeO_3$;BY: $BiYO_3$;

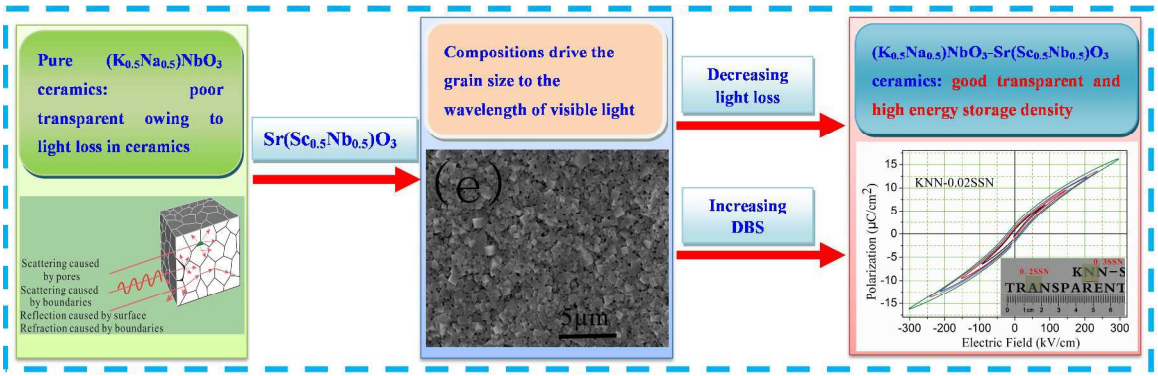

Figure 1 Schematic diagram of increasing optical transparency and energy storage density by decreasing the grain size through compositions driven.

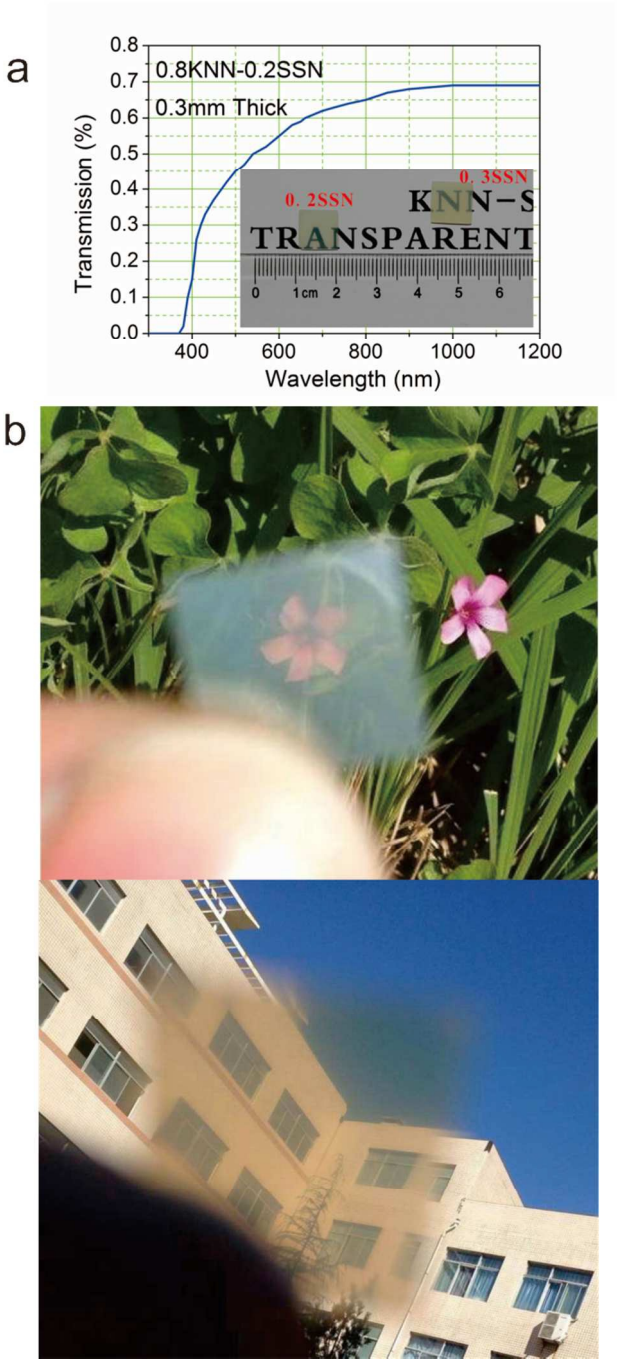

Figure 2 Transparency of the (1-x)KNN-xSSN ceramics. (a) Transparency of the 0.8KNN-0.2SSN ceramics polished to a thickness of 0.3 mm. The lower-right inset shows sample photo of the transparent 0.8KNN-0.2SSN and 0.7KNN-0.3SSN ceramics. (b) Photograph of a visibly transparent 0.8KNN-0.2SSN ceramics.

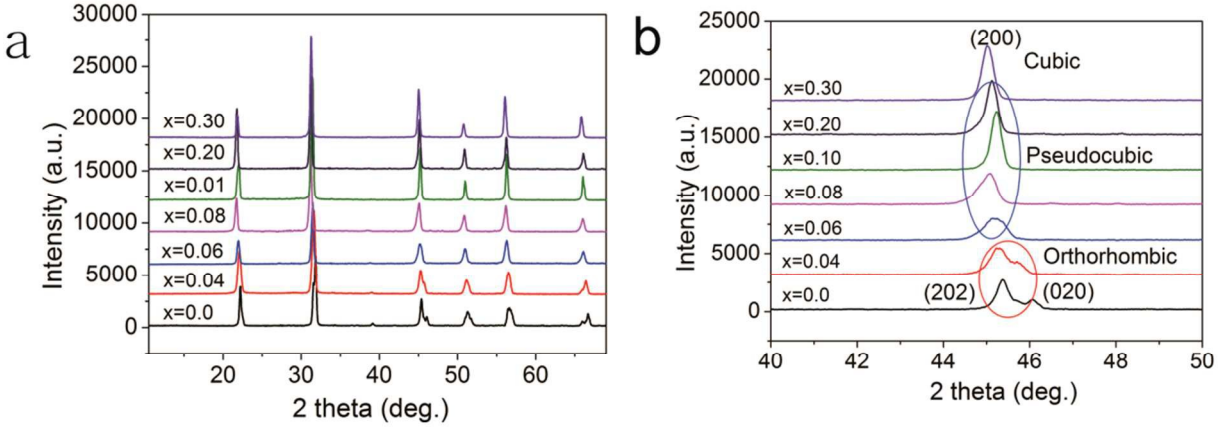

Figure 3 XRD patterns of the (1-x)KNN-xSSN ceramics. (a) XRD patterns and (b) expanded XRD patterns (40°~50°)

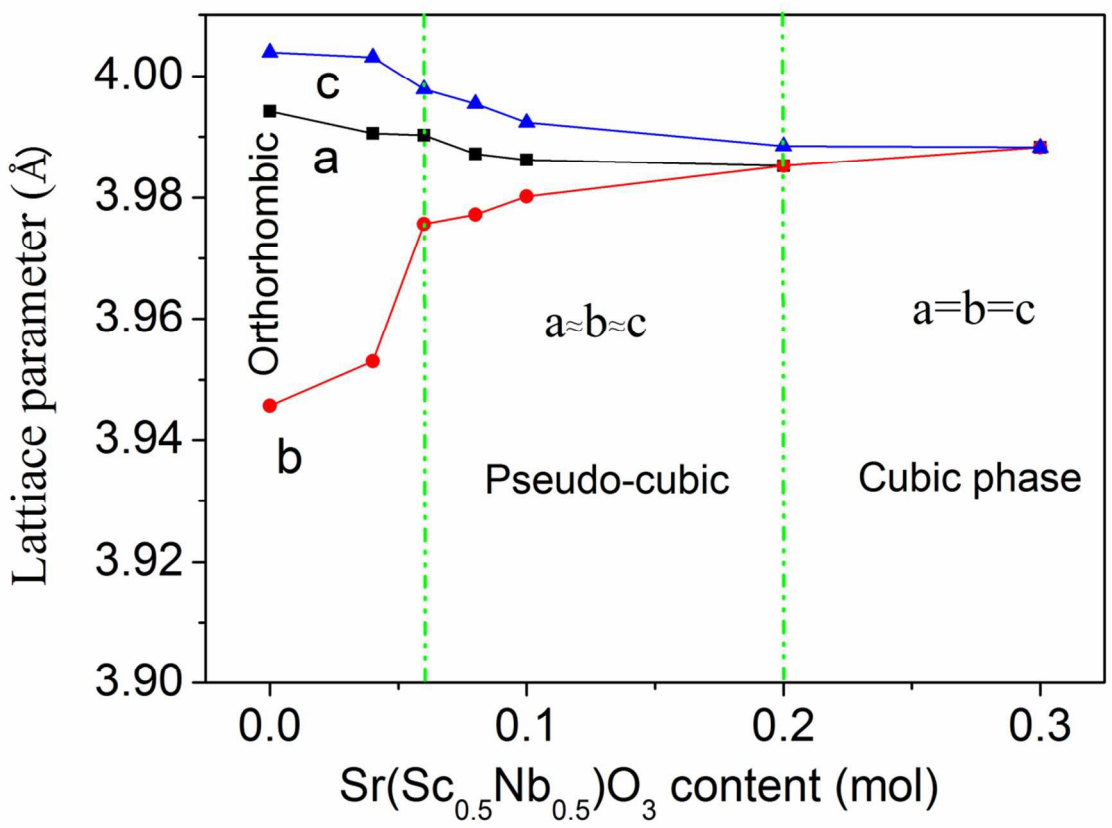

Figure 4 Lattice parameters of (1-x)KNN-xSSN ceramics as a function of x.

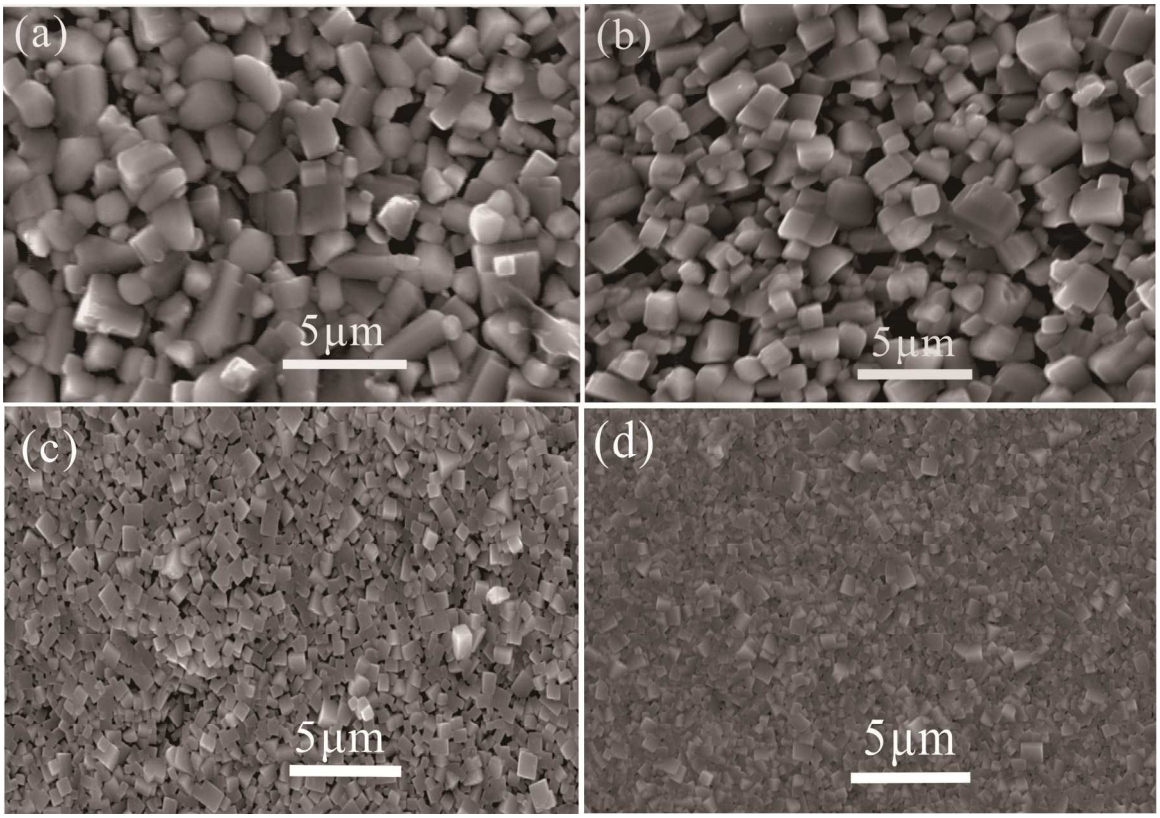

Figure 5 SEM images of the (1-x)KNN-xSSN ceramics with (a) x=0; (b) x=0.04; (c) x=0.2; (d) x=0.3;

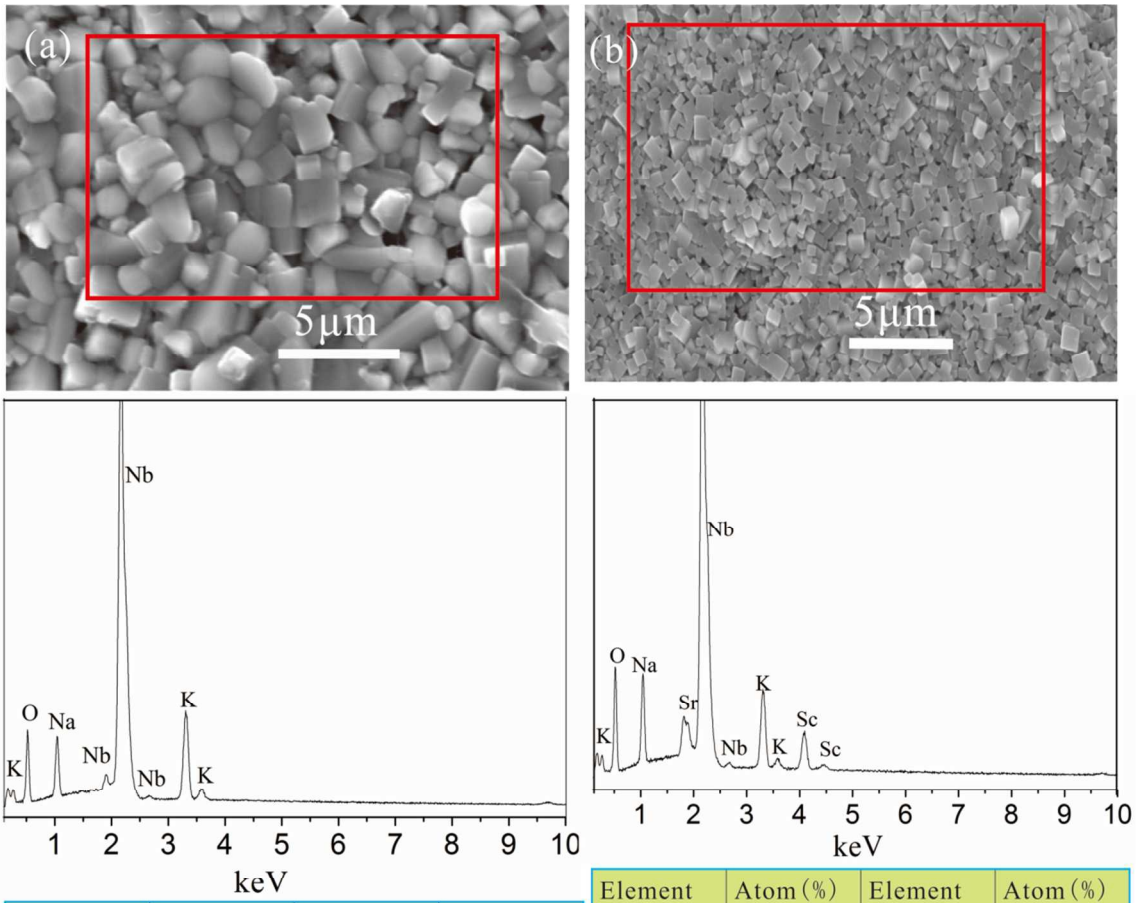

Element	Atom (%)	Element	Atom (%)
O	59.48	K	8.73
Nb	22.11	Na	9.68

Element	Atom (%)	Element	Atom (%)
O	58.85	K	7.25
Nb	20.11	Sr	3.87
Na	7.82	Sc	2.10

Figure 6 Surface morphologies, EDS spectra, and atomic percentages of the elements of 0.8KNN-0.2SSN

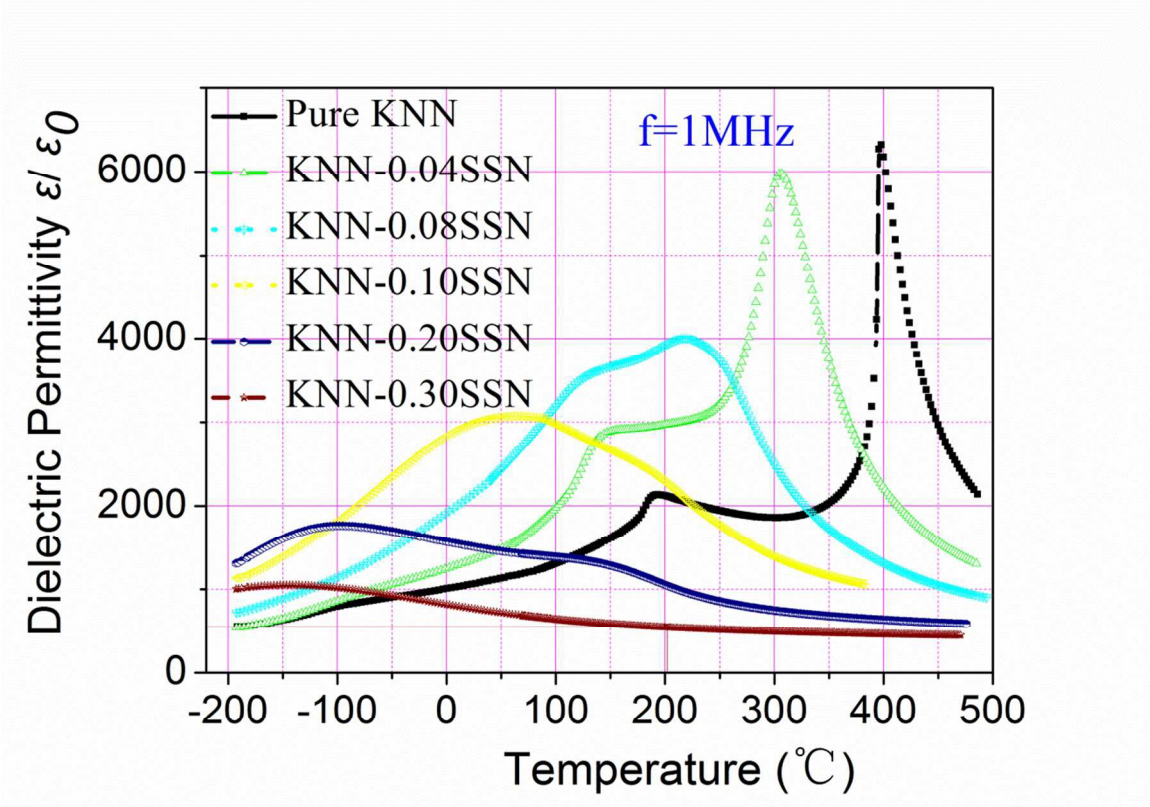

Figure 7 Temperature dependence of dielectric permittivity of (1-x)KNN-xSSN ceramics within a temperature range of -193-500 °C.

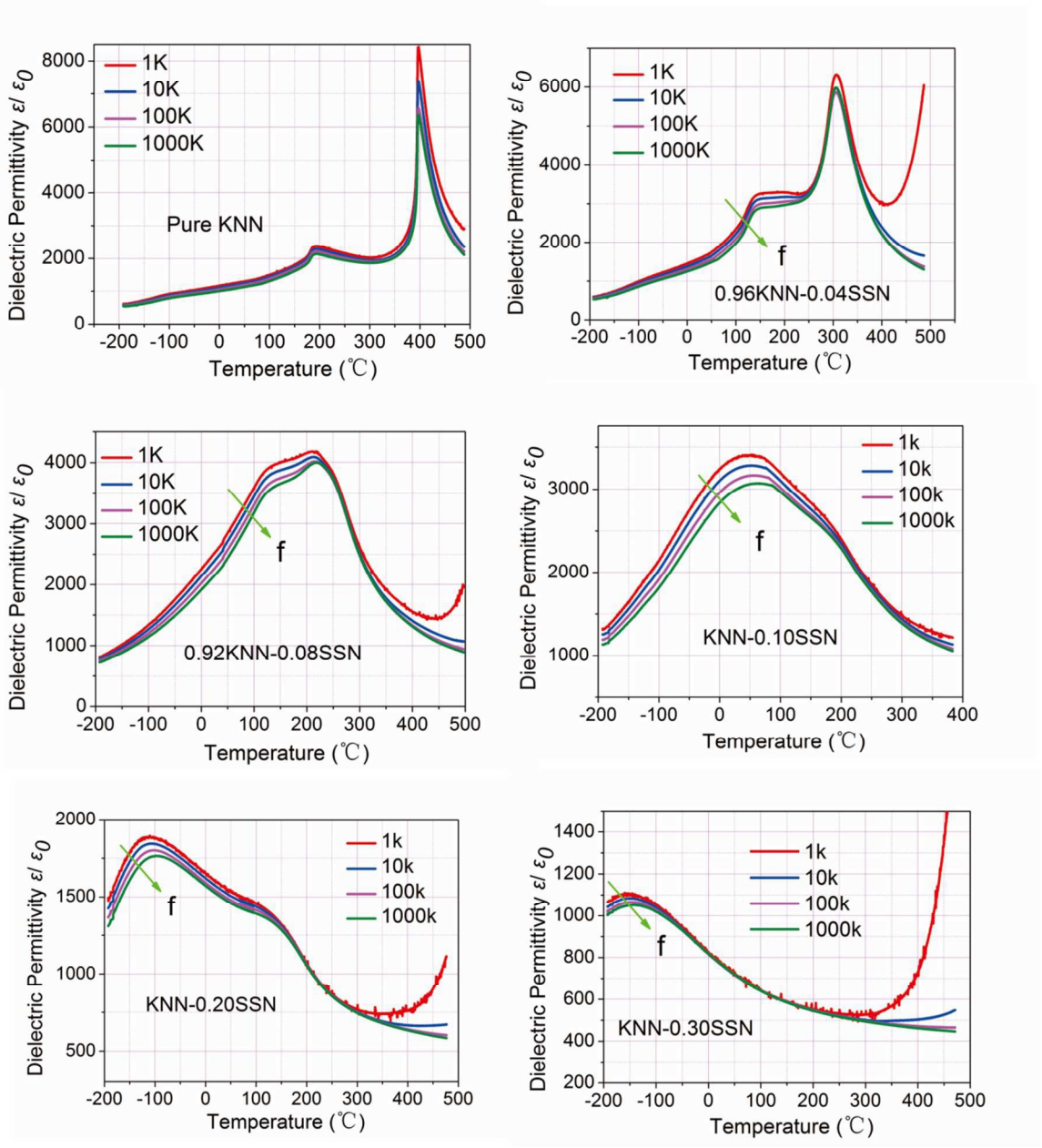

Figure 8 Temperature dependence of dielectric permittivity of (1-x)KNN-xSSN ceramics at various measuring frequencies.

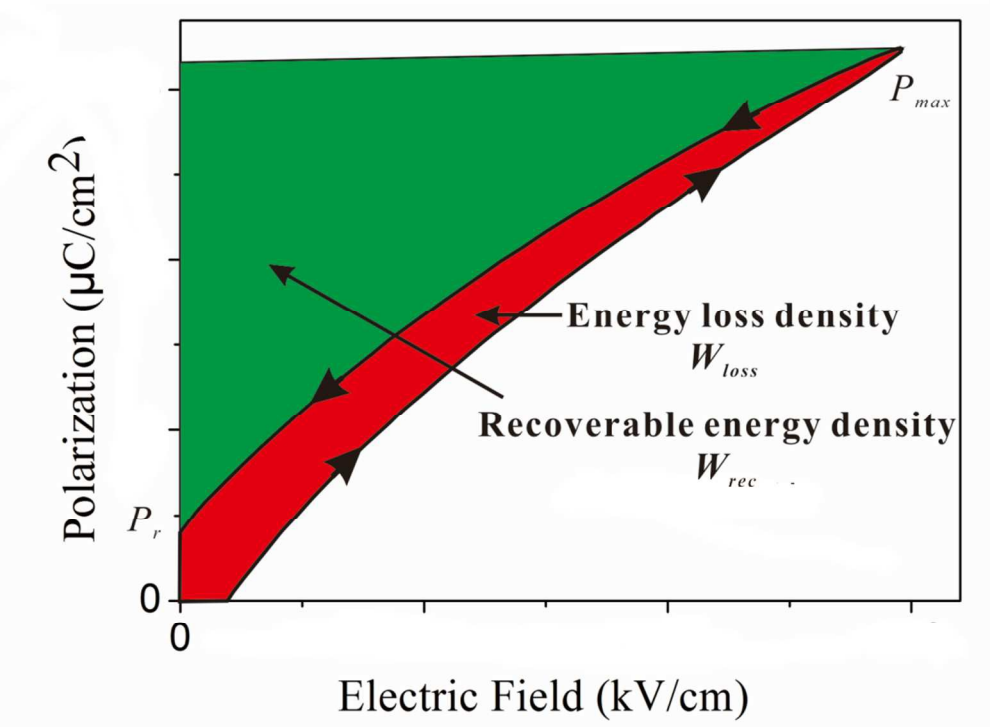

Figure 9 Schematic calculations of energy storage properties of relaxor ferroelectric materials.

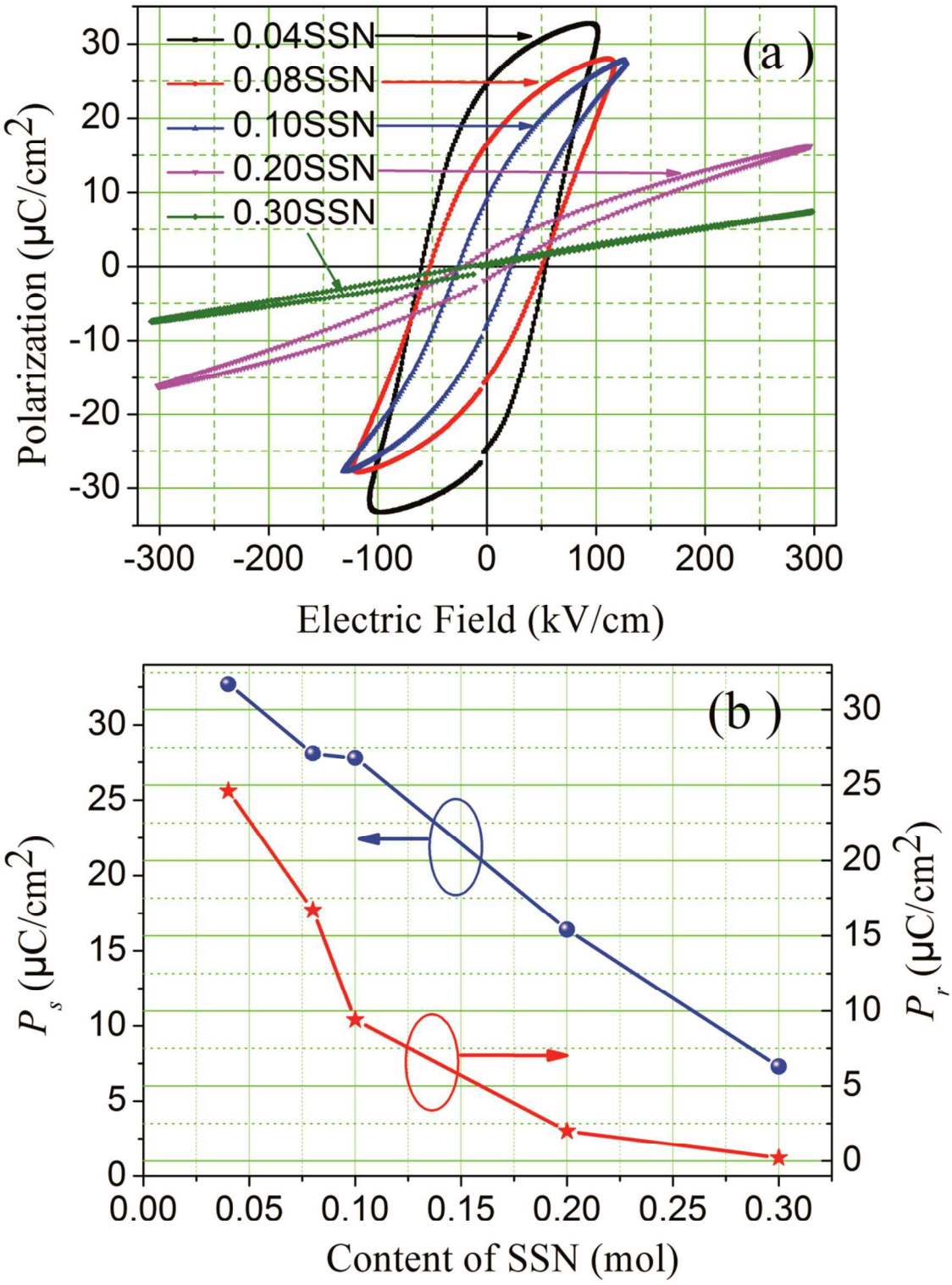

Figure 10 (a) P–E hysteresis loops at their critical breakdown strength for (1-x)KNN-xSSN ceramics; (b) P_s and P_r of (1-x)KNN-xSSN ceramics.

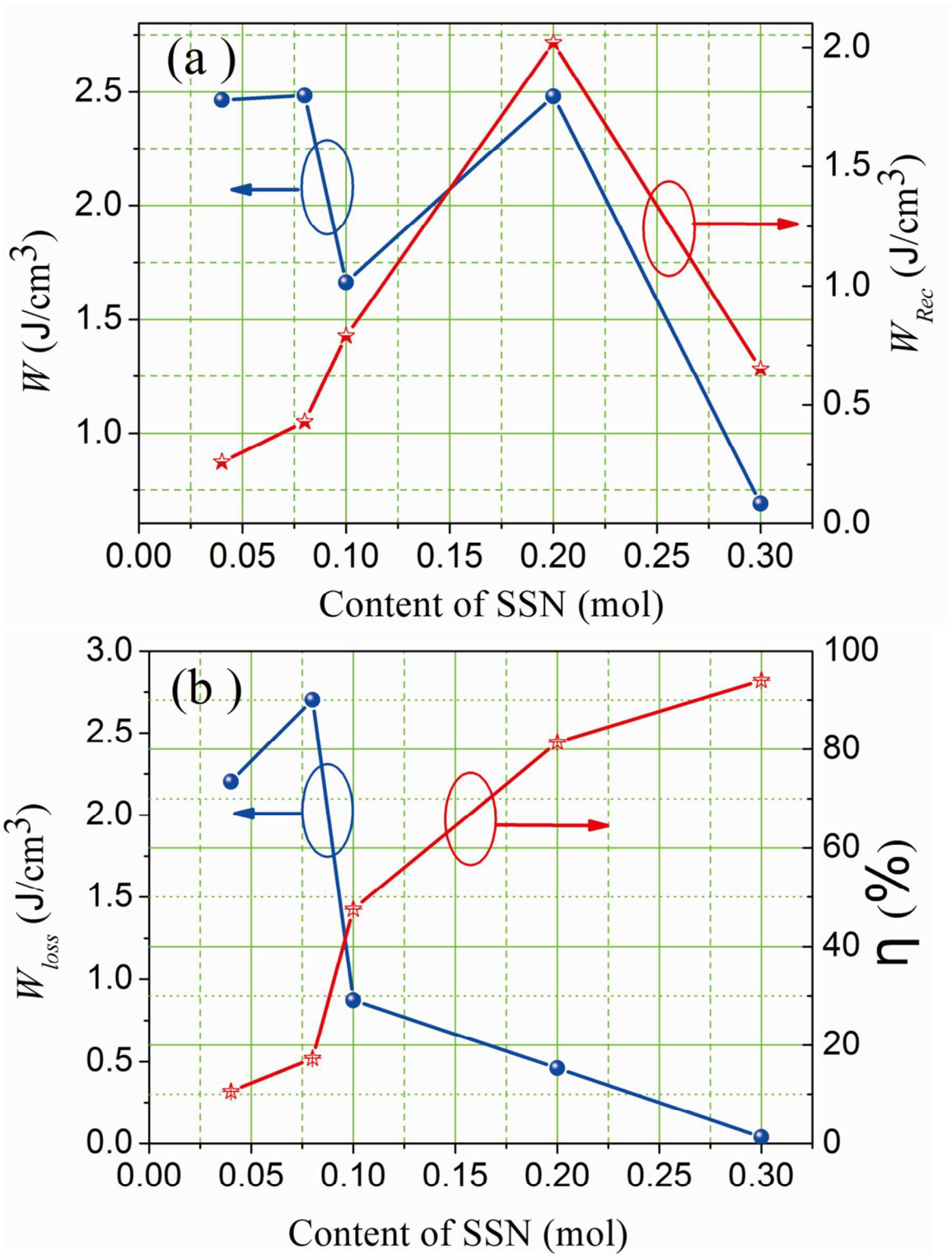

Figure 11 (a) The calculated energy storage density W and the recoverable energy storage density W_{rec}; (b) The calculated energy loss density W_{loss} and the energy storage

efficiency η.

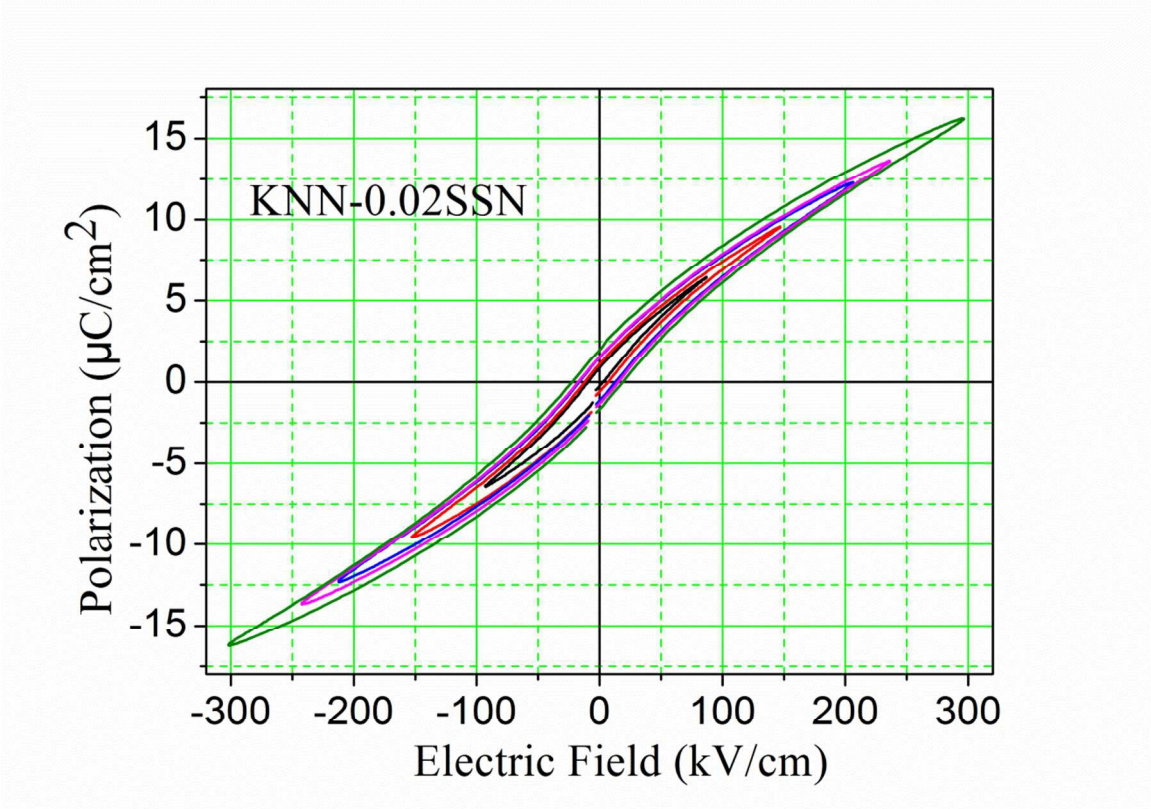

Figure 12 Variations of P–E hysteresis loops of 0.80KNN-0.20SSN ceramics at room temperature under different electric fields.